



High Performance Dye Sensitized Solar Cells by Plasmonic Enhancement of Silver Nanoparticles in ZnO Photoelectrode with Betanin Pigment

Eli Danladi^{a,*}, Muhammad Y. Onimisi^b, Reuben M. Laah^b, Imosobomeh L. Ikhioya^c

^aDepartment of Physics, Faculty of Science, Federal University of Health Sciences, Otuopko, Benue State, Nigeria

^bDepartment of Physics, Faculty of Science, Nigerian Defence Academy, Kaduna, Kaduna State, Nigeria

^cDepartment of Physics and Astronomy, Faculty of Physical Sciences, University of Nigeria, Nsukka, Enugu State, Nigeria

Abstract

Metal nanoparticles (NPs) introduced in sensitive places in Dye Sensitized Solar Cells (DSSCs) has demonstrated superior performance due to surface plasmon resonance effect. Herein, a systematic investigation by introducing plasmonic silver nanoparticles (AgNPs) in the photoanode of DSSCs with Zinc oxide (ZnO) is investigated. The broadening of the absorption band in the visible region is made possible using the natural pigments betanins. The combined effect of UV-visible absorption spectroscopy, XRD technique, SEM and solar simulator were used to explore the surface plasmon resonance effect. The ZnO photoanode without AgNPs shows a Power Conversion Efficiency (PCE) of 0.156 %, Current Density (J_{sc}) of 0.477 mAcm^{-2} , Open Circuit Voltage (V_{oc}) of 0.762 V and Fill Factor (FF) of 0.431. On coating AgNPs on the pristine photoanode, the PCEs were improved significantly as compared with the pure ZnO based device. The AgNPs were deposited in cycles (2 cycles, 4 cycles and 6 cycles). The device with 2 cycles of Ag NPs, shows a PCE of 0.373 % which demonstrates an enhancement of ~ 2.39 times to that of the pristine device. Also depositing 4 cycles of AgNPs results to PCE of 0.290 % which shows a leading of 0.134 % ahead of the reference PCE. With 6 cycles of AgNPs deposited on the photoanode of bare ZnO NPs, it results to PCE of 0.244%, FF of 0.592, J_{sc} of 0.572 mAcm^{-2} and V_{oc} of 0.722 V which also shows an enhancement of ~ 1.56 times, ~ 1.37 times and ~ 1.20 times in PCE, FF and J_{sc} over the device lacking AgNPs. These results show significant increment in performances of all the devices with silver inclusion. The performance is attributed to the reduced recombination of electron-hole pairs due to the Ag-ZnO junction and the generation of intense electric fields at the immediate vicinity of the sensitizer, resulting in enhanced light absorption.

DOI:10.46481/asr.2022.1.1.3

Keywords: Betanin, Plasmonic, DSSC, Nanoparticle

Article History :

Received: 04 December 2021

Received in revised form: 05 February 2022

Accepted for publication: 07 February 2022

Published: 29 April 2022

© 2022 The Author(s). Published by the Nigerian Society of Physical Sciences under the terms of the Creative Commons Attribution 4.0 International license. Further distribution of this work must maintain attribution to the author(s) and the published article's title, journal citation, and DOI.

Communicated by: Babatunde J. Falaye

1. Introduction

Dye-sensitized solar cells that mimic photosynthesis has been completely redesigned, and prototypes have been created to replace expensive silicon solar cells. DSSC was developed in the early 1990s, which is based on dye sensitization of a wide bandgap nanostructured semiconductor. Because transition metal coordination compounds (for example, ruthenium polypyridine complexes) have strong absorption, long excitation lifetime, and effective metal-ligand charge transfer in the visible region of the spectrum, they were employed as sensitizers in DSSCs [1]. The use of synthetic dyes leads to high production costs and sometimes has a negative impact on the environment. These results have prompted researchers to look for cheaper and more environmentally friendly alternative dyes. Natural pigments, including lawsome [2], chlorophyll [3, 4] carotene [2, 5, 6], betanin [2, 7], betalain [4, 6, 8-10], anthocyanin [6, 9, 11, 12, 13, 14] etc., are freely available in plant leaves, flowers, and fruits and have been used to fulfill the requirements of sensitizers. To date, average efficiencies achieved for natural DSSCs are ~ 0.4%, with the highest being ~ 1.5 – 2.0% [2]. Most photoanodes that are used in DSSCs are made of semiconductor materials such as TiO₂ [2, 11, 15, 16, 17], SnO₂ [18], ZnO [1, 19, 20, 21], Nb₂O₅, SrTiO₃, Fe₂O₃, WO₃ and Ta₂O₅ [20]. Amongst the listed of them all, zinc oxide has shown some attracted properties that made it candidate of choice, such as high electron mobility of 115-155 cm² V⁻¹ s⁻¹, stability against photocorrosion, large excitation binding energy (60 eV) and band gap near the one of TiO₂ [20, 21]. Besides, ZnO is found at low-cost and in many forms, like nanorods, nanowires and nanosheets [22]. However, DSSCs employing ZnO has demonstrated lower PCE. Some reasons attributed to this are insufficient attachment of natural dyes with the nanoparticles, formation of aggregation between the nanoparticles up on film formation, low injection rate, low regeneration of electron, and formation of Zn²⁺/dye complex [1]. Therefore, modifying ZnO surface will reduce the aggregation of dye molecules which subsequently will minimize the rate of recombination for it to appear as a high device PCE in the horizon of photovoltaics.

Here, we propose a method to sensitize ZnO photoelectrodes with betanin pigments from *Beta vulgaris* after introducing AgNPs cycles, which can demonstrate surface plasmon resonance effects. The effect of surface plasmon resonance will be manifested through the coupling of near-electromagnetic fields [23, 24]. In this case, the metal nanoparticles will generate a strong electric field on the surface, which is several orders of magnitude stronger than the incident light. They will combine with sensitizers in close proximity, resulting in increased light absorption.

2. Materials and Methods

2.1. Preparation of the Natural Dye

Betanin pigment was extracted from beetroot (*Beta vulgaris*) using water as the solvent as follows: 165 ml of water was added to 66.198 g of *Beta vulgaris*. The mixture was blended using an electric blender as shown in Figure 1a. The resulting liquid was filtered to obtain the pure dye solution which was used as our sensitizer. The chemical structure of the dye is as shown in Figure 1b [2].

2.2. Preparation of the Electrolyte

The electrolyte used in this research work is an iodide-based liquid electrolyte. It was prepared using a method earlier described by Danladi *et al.*, Mphande *et al.* and Jun *et al.* [25, 26, 27]. It involves mixing 0.6 M 3-propyl-1-methylimidazolium iodide, 0.1 M lithium iodide, 0.05 M iodine and 0.5 M 4-tert-butylpyridine in acetonitrile.

2.3. Preparation of ZnO nanoparticles

Zinc chloride (ZnCl₂) and sodium hydroxide (NaOH) were the precursors for the ZnO nanoparticles formation.

An analytical scale balance was used to measure ZnCl₂ and NaOH in grams in the ratio 1:8. The choice of the ratio is based on the fact that higher concentration of alkaline compound (NaOH) facilitates the formation of ZnO [28, 29]. The constituents which are of analytical standards were transferred into a beaker containing 700 ml of ethanol which serves as the reaction solvent. The ethanol was added dropwise until it reaches 1000 ml. A white precipitate

*Corresponding author tel. no: +2348063307256

Email address: danladielibako@gmail.com (Eli Danladi)

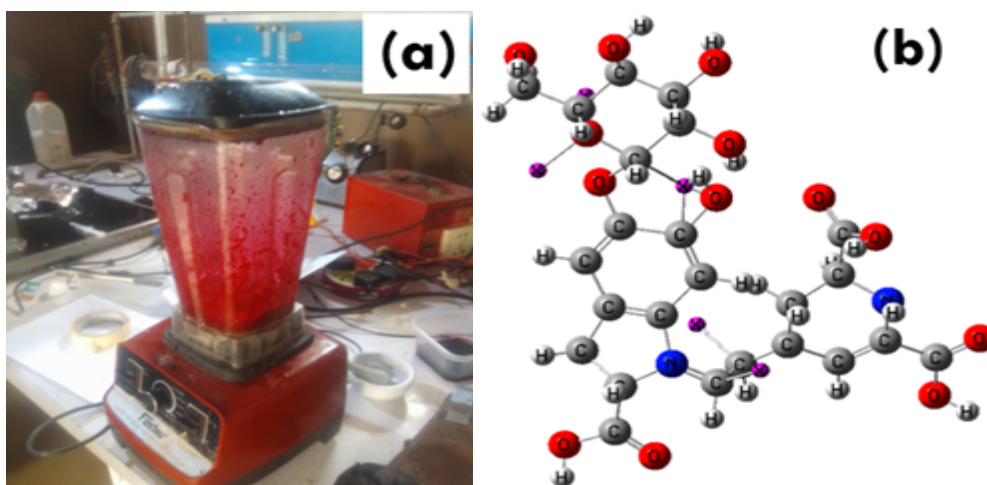


Figure 1: (a) Extraction process of betanin from beetroot, and (b) 3D molecular structure of betanin [2].

was immediately formed in the mixture which was kept under vigorous stirring at room temperature for 20 minutes. The white precipitate was filtered and washed using deionized water and thereby redispersed with an adjustable PH between 8-9 in the presence of hydrochloric acid (HCl) in drops. The mixture was additionally stirred with the help of a magnetic stirrer (78-1 PEC medical, USA) for 3 hours. It was transferred into Teflon-lining of a hydrothermal autoclave and heated in a hot air oven at 190 °C for 5 hours. Once heat treatment of the sample was achieved, the oven was allowed to cool to room temperature. The sample was placed in a crucible at 80 °C for another 5 hours.

2.4. Preparation of AgNPs

To fabricate the silver NPs, a modified two-step reduction synthesis procedure was implemented, which was developed based on the conventional reduction method [30, 31]. The mixture containing sodium borohydride (NaBH_4) and tri-sodium citrate (TSC) was first heated at the ratio 2:7 to 60 °C at 300 rpm for 30 minutes under vigorous stirring to ensure a formation of homogenous solution. 45 minutes later, 4 ml of an aqueous solution of AgNO_3 (4×10^{-3} mol dm^{-3}) was added drop-wise to the mixture, and the temperature was further raised to 100 °C to make the solution boil quickly. The reaction proceeded for another 45 minutes. Finally, the solution was cooled to room temperature with stirring, and the NPs were collected by centrifugation at 4000 rpm and redispersed in ethanol via sonication for 15 minutes.

2.5. Preparation of the solar cell photoanodes

Fluorine-doped tin oxide (FTO) substrates with dimension of 15 mm \times 15 mm \times 2 mm; sheet resistance 15 Ω square⁻¹ were thoroughly cleaned with cotton wool and ethanol. It was then sonicated for 2 minutes to remove impurity. ZnO film was dispersed on the FTO to form the compact layer using doctor blade method, followed by dispensing the meso-ZnO nanoparticles form in section 2.3, using spin coating technique for 10 seconds at a rotational speed of \sim 3000 rpm. It was subsequently annealed at 450 °C for 45 minutes. The three photoanodes with AgNPs were formed by coating 2 cycle, 4 cycle and 6 cycle on the AgNPs on the nanoparticle scaffold. Thereafter, a thin layer of Zirconium was used as an insulating shell for stability.

For the pristine device, the photoanode was prepared by coating pure ZnO and annealed under the same conditions mentioned for the plasmon-solar cells. The betanin pigment was impregnated on the different photoanodes and left immersed for 24 hours under dark condition. The soaked nanoparticles were gently rinsed with ethanol to remove residue and dried at room temperature. To ensure good device performance, pre-and-post TiCl_4 treatment of the photoanodes was done as described by Sreeja and Pesala [2], Danladi et al. [25], Sandquist and McHale [7]. A spacer with a thickness of 30 μm was created around the coated portion of the photoelectrodes. This spacer will hasten the liquid electrolyte to fill up to the maximum thickness (30 μm) required for the electrolyte and also protect the ZnO-coating-free portion of the FTO substrate from short-circuiting on contacting the counter electrode.

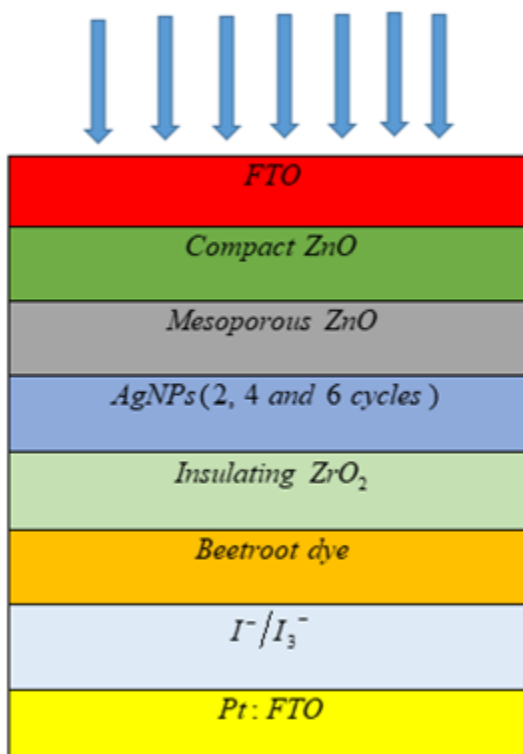
Direction of incident solar spectrum

Figure 2: Illustration of the anthocyanins-betalains sensitized solar cell with AgNPs incorporated in the photoanode.

2.6. Preparation of the counter electrodes

The counter electrode was prepared by spin coating a platisol catalyst, purchased from solaronix on FTO for 20 seconds at 3000 rpm. The Pt coated FTO was then sintered at 500 °C for 30 minutes.

2.7. DSSCs Assembly

The Platisol counter electrode is assembled over the photoanode to build a standard DSSC sandwiched–configuration. The electrolyte is injected into the solar cell assembly via a 0.5 mm diameter hole drilled in the counter electrode and thereafter sealed. The solar cells active area was 1 cm². The DSSCs fabrication process was performed at room temperature and ambient laboratory conditions. The schematic of the cell is as shown in Figure 2.

2.8. Characterization and measurement

The surface morphologies were observed by Scanning Electron Microscopy (Phenom Pro X model, Eindhoven de Netherlands). The SEM observations were made with acceleration voltage of 15 kV. At that point, we utilized ISO-lution Image Analysis programming to measure the size of Ag nanoparticles that was deposited on the ZnO to be 5 nm.

Structural analyses of the fabricated films were performed using X-ray diffractometer (XRD, Rigaku D, Max 2500, Japan).

Optical spectra were characterized using ultraviolet–visible light (UV–vis) spectrometer (Axiom Medicals UV752 UV-vis-NIR), FT-IR spectrometer (Agilent Technologies) was used to study the functional groups.

X-ray microanalysis of the elemental composite layer was carried out with INCA EDX analyzer by bombarding with a finely engaged (<10 nm measurement) electron beam with an acceleration voltage of 10-150 kV under vacuum.

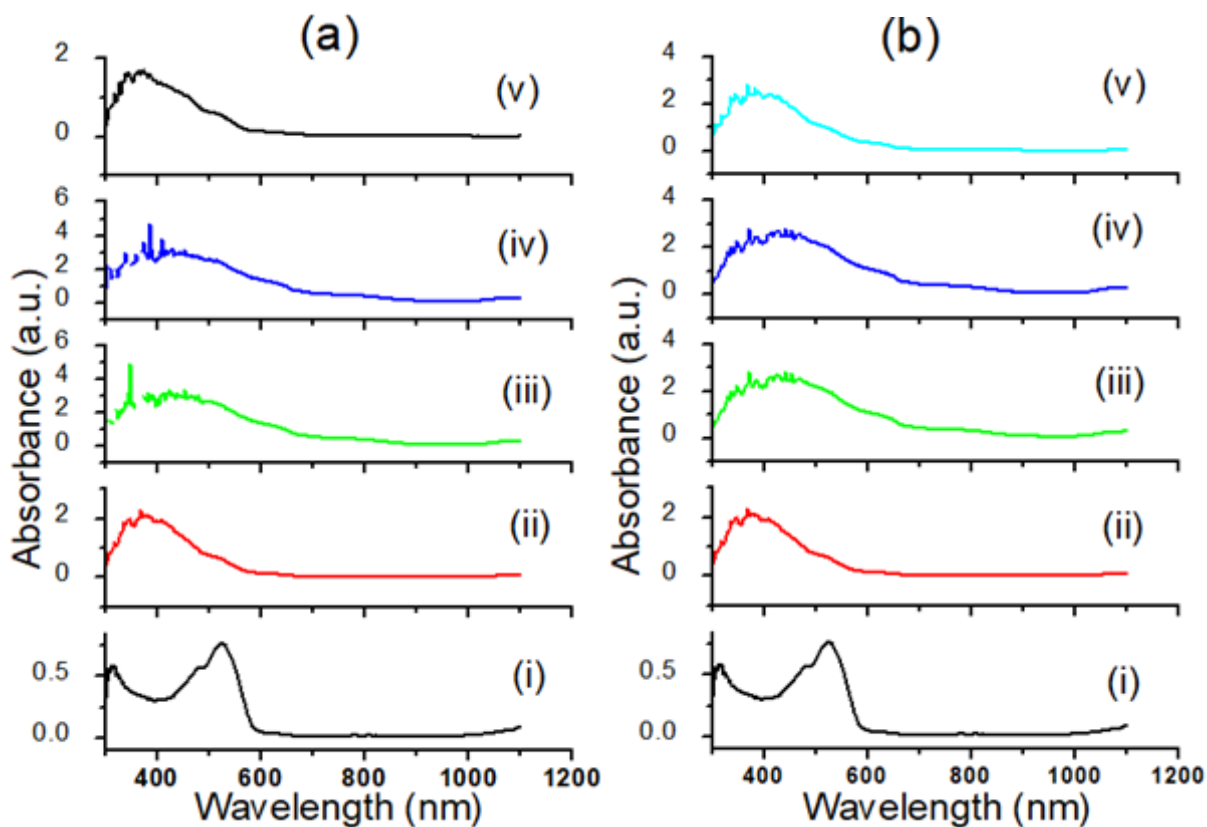


Figure 3: Absorbance-wavelength of (a) dye and various photoanodes without dye, (b) dye and various photoanodes with dye.

The current density-voltage performance of the DSSCs were estimated using a solar simulator (Newport Corporation) and a Keithley 2400 (Keithley, Inc.) source-meter. The performance characteristics of the solar cells were evaluated under 1 sun illumination (AM 1.5G standard test conditions at 100 mWcm^{-2}).

3. Results and Discussion

3.1. Ultraviolet-Visible-Infrared Absorption Studies

The absorbance spectra of the dye and various photoanodes are shown in Figure 3. The absorbance study was carried out within the wavelength range of 300 to 1200 nm. The beetroot is rich with betanin pigment. The absorption peak of betanin pigment was detected at 530 nm at an absorbance of 0.801 a.u which is typical of betanin [2, 32] and agrees with similar peaks in literatures [2, 33, 34, 35]. The observed peak is attributed to the excitation of electrons from the highest occupied to the lowest unoccupied molecular orbital that takes place between the betaine moiety and betalamic acid of the betanin molecule [2]. The pair of nonbonding electrons located on the N-atom of the betaine moiety undergoes delocalization with the electrons located on the conjugated π systems. The subsequent $n \rightarrow \pi^*$ transitions result in the absorption of electromagnetic radiation in the green wavelength range [2].

The optical absorbance spectra of ZnO and ZnO/Ag with and without betanin pigment is shown in Figures 3a&b(ii-v). An absorbance band with peak at 377 nm was observed for ZnO in the optical spectra (Figure 3a(i)) and it indicates good crystallinity of the film. After loading the dye, good quality absorbance in the entire visible range with broader peak for ZnO was observed (Figure 3b(ii)). The absorption of ZnO was shifted towards higher wavelength, this shows that in the presence of betanin pigment, the ZnO have a broader absorption capacity than in its absence. Incorporation of AgNPs in the photoanodes further increases the absorbance of ZnO film as shown in Figure 3a(iii-v). For the solar

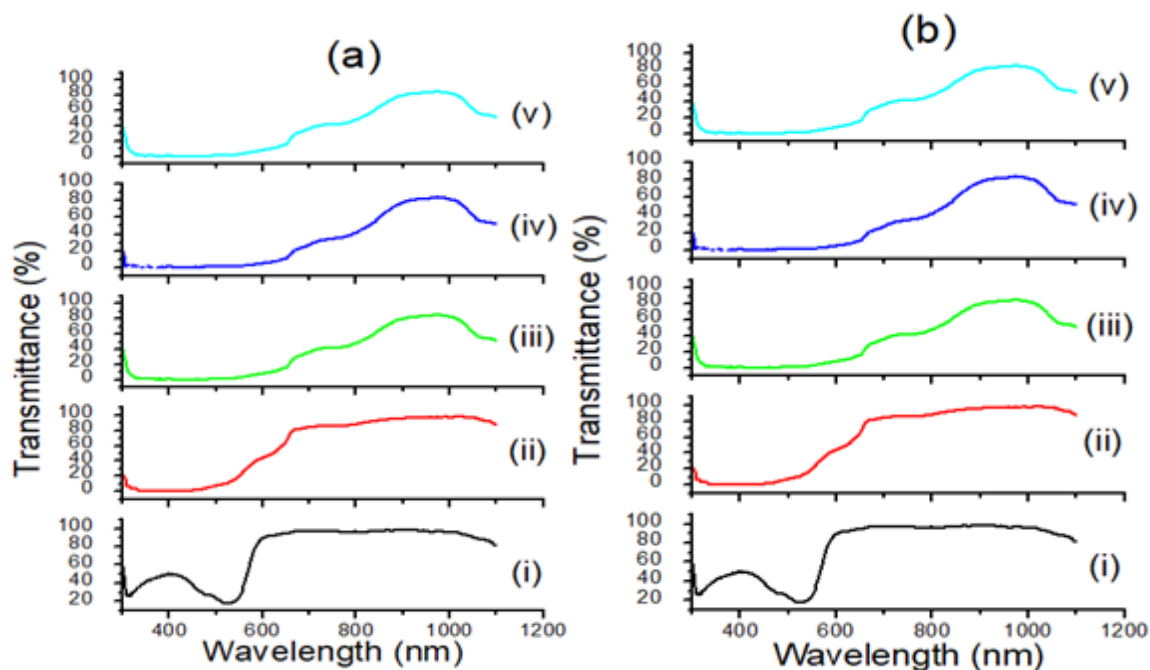


Figure 4: Transmittance-wavelength of (a) dye and various photoanodes without dye, (b) dye and various photoanodes with dye.

cells with silver nanoparticles to notice a significant enhancement over the device lacking AgNPs, the absorption peaks of the pigments in the photoanode must match the plasmonic scattering peaks of the incorporated AgNPs [2]. The changes in absorption of the AgNPs incorporated photoanodes are shown in Figure 3b(iii-v). The relatively broad and strong enhancement is observed in the range of 380–650 nm, which falls within the Localized Surface Plasmon Resonance (LSPR) band position of decorated AgNPs. This enhanced absorption and broadened spectra absorption range of the photoanodes were mainly attributed to the Surface Plasmon Resonance of Ag-NPs [36]. These features suggest that dye molecules in the vicinity of AgNPs can absorb more photons, presumably due to the intensified near-field effect of the surface plasmon and spectral overlap between the dye and surface plasmon, which may eventually lead to an increase in the number of charge carriers and J_{sc} values. The ZnO, ZnO/2Ag, ZnO/4Ag and ZnO/6Ag was red shifted from 377 to 385 nm, 438 to 452 nm, 431 to 451 nm, 365 to 388 nm when betanin molecule was added. This studies demonstrates the importance of using natural pigment for activation of semiconductors for photovoltaic applications.

3.2. Transmittance Studies

Figure 4 compares the optical transmission of the different as-prepared photoanodes with dye and without dye. A spectrum without nanoparticles is also included for reference. At wavelengths between 550 nm and 1050 nm, all samples incorporating AgNP were observed to have lower transmittance than the reference sample (ZnO). This is due to the dispersion of light at various interstitial layers present in the formed films [37].

The band peak from modified sample was observed around 970 nm. There was also a broaden behavior in the spectra that results to redshifting when the various photoanodes are soaked in the betanin pigment. The observed differences in the transmittance of the film can be attributed to the presence of surface defects, which results in inconsistencies in surface morphology, crystal size, and transmittance to light scattering. The enhancement can be related to the excited SPR from AgNP. The bonding strength between the surface plasmons of metal nanoparticles depends on the scattering of the AgNPs, the field-bonding of the dielectric nanoparticles to the ZnO substrate, or the combination of metal and dielectric particles [37].

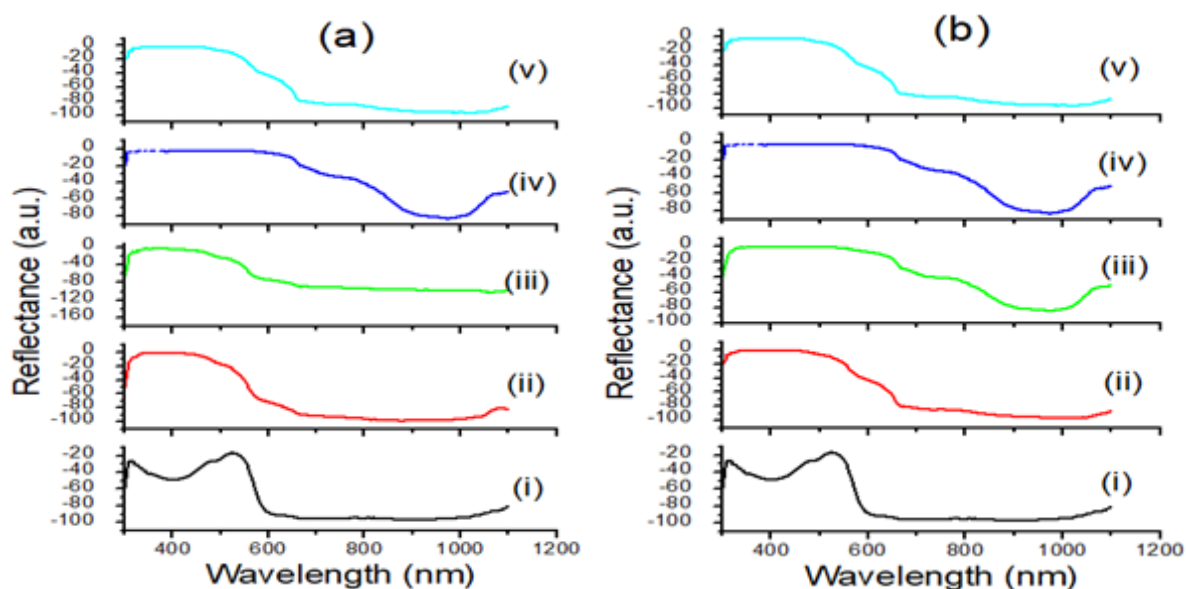


Figure 5: Reflectance-wavelength of (a) dye and various photoanodes without dye, (b) dye and various photoanodes with dye.

3.3. Reflectance Studies

From the plots (Figure 5), we observed a strong scattering contribution (reflectance) from AgNP clusters within the range of 300-1200 nm. The result of strong local fields produced by NP interactions is also expected to partially offset the lower radiation efficiency of isolated NPs [38].

The redshift and broadening of the main scattering band are due to the random aggregation of the dispersed nanoparticles forming clusters [39,40]. However, as shown by the films with different cycle of AgNPs, the measured reflectance spectra show peaks and valleys.

3.4. Fourier Transform Infrared studies

Figure 6 shows the FTIR result for dye extract and ZnO NPs synthesized by the extract.

As observed in the dye spectrum, a broad peak ranging from $3200\text{--}3650\text{ cm}^{-2}$ at peak intensity of 3257.7 cm^{-1} is attributed to the hydroxyl functional group, a second peak ranging between $1650\text{--}1850\text{ cm}^{-1}$ at peak intensity of 1636.3 cm^{-1} is assigned to the stretching of the carbonyl functional group of a carboxylic acid.

As observed in the spectrum of ZnO with dye extract, the band at 2929.7 cm^{-1} corresponds to the carbon-hydrogen unit. The intense bands at 868.5 and 710.0 cm^{-1} are due to stretching vibration modes of Zn-Cl units [41]. The very weak peak at about 1013.8 cm^{-1} are due to nitrate groups and correspond to their asymmetric and symmetric stretch and deformations of zinc carboxylates [28, 41, 42] resulting in the participation of carboxylic group of the beetroot dye. The band at 1651.2 cm^{-1} is attributed to Carbonyl group. The band at 2118.4 cm^{-1} is ascribed to the alkyne group unit. When the two spectra are compared, there were absence of some peaks and other new peaks were introduced in the spectrum of ZnO soaked in the betanin pigment. This is due to the ability of the extract to act as reducing agent in the presence of the nanoparticles.

3.5. Structural Studies of Chemically Synthesized ZnO Nanoparticles

The XRD pattern for ZnO is as shown in Figure 7. The diffraction peaks at 2θ values were observed at 31.19° , 33.76° , 35.65° , 46.96° , 56.09° , 62.33° and 67.49° for the ZnO film and correspond to (100), (002), (101), (102), (110), (103) and (112) respectively, which shows the characteristic of the hexagonal structure of ZnO nanoparticles in accordance with JCPDS Card No. 80-0075.

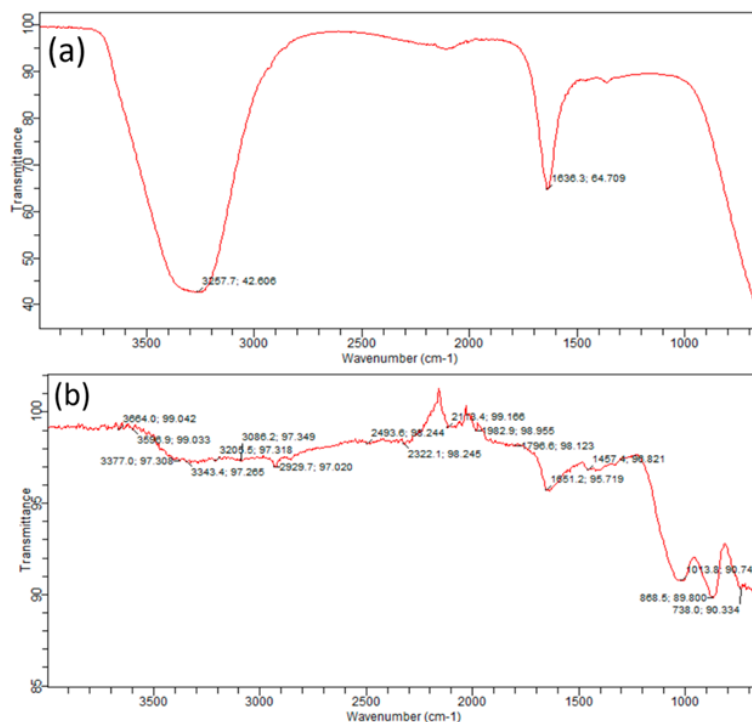


Figure 6: FT-IR spectra of (a) dye and (b) ZnO nanoparticles synthesized by dye extract.

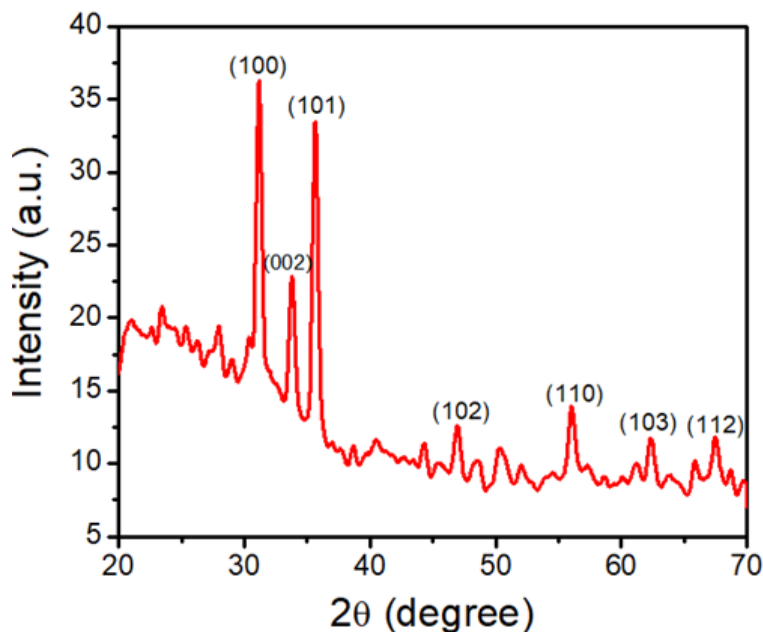


Figure 7: The XRD patterns of ZnO.

3.6. Scanning Electron Microscope (SEM)

Information regarding the surface structure of the films was obtained from the SEM studies where the surface structure was probed using electrons that penetrated into the sample. This provided a resolution.

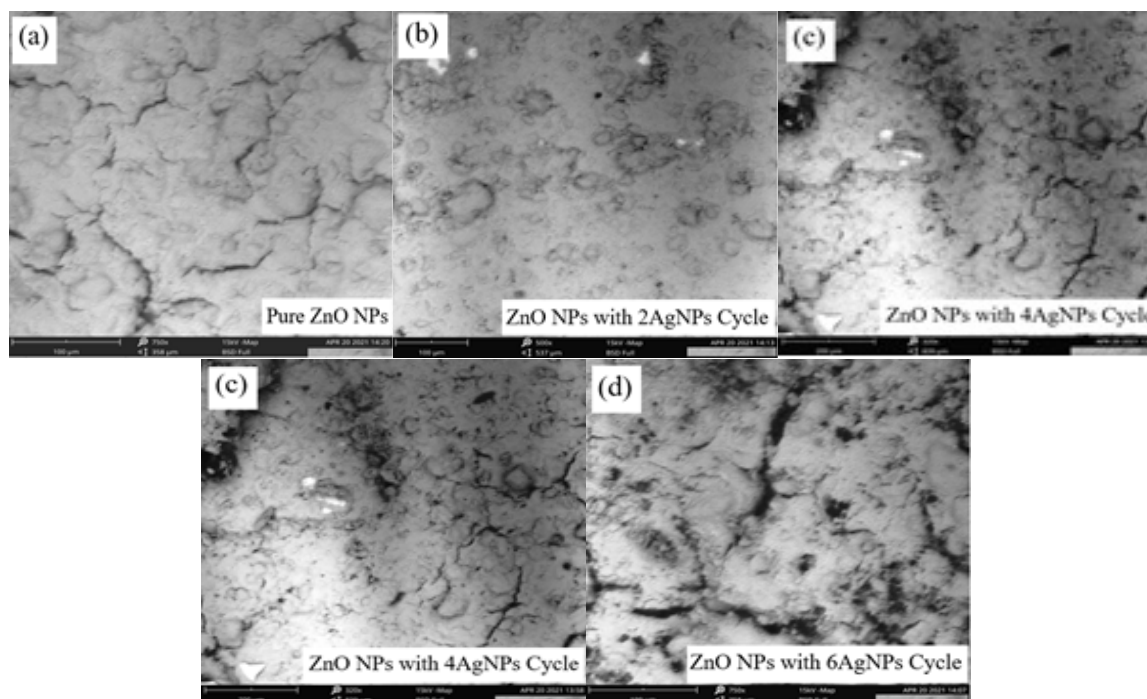


Figure 8: SEM images of (a) the pure ZnO, (b) ZnO with 2AgNPs cycle, (c) ZnO with 4AgNPs cycle, (d) ZnO with 6AgNPs cycle and (e) AgNPs.

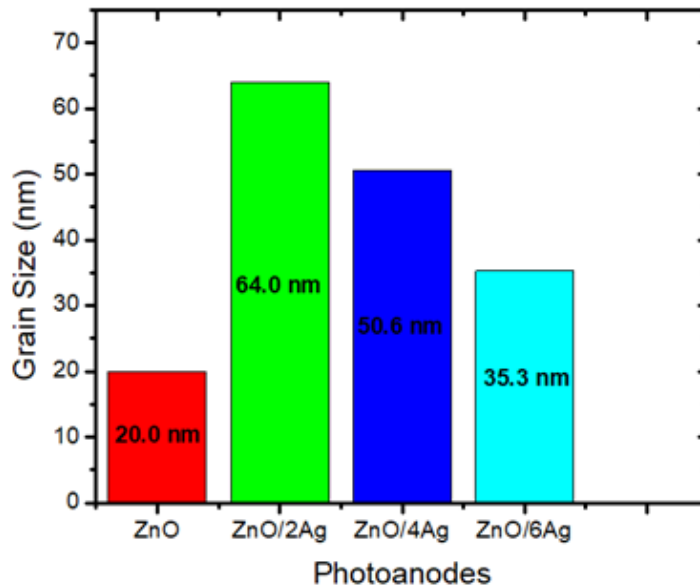


Figure 9: The plot of Grain Size versus Photoanodes of (a) the pure ZnO, (b) ZnO with 2AgNPs cycle, (c) ZnO with 4AgNPs cycle, and (d) ZnO with 6AgNPs cycle.

The image presented as Figure 8 is the SEM images of as-synthesized ZnO and Ag–ZnO samples with varying cycle of silver nanoparticles. The presence of aggregated spherical particles, with an average size of ~32 nm as obtained from Isolution image analyser programming can be seen in the SEM image (Figure 8a) of the pristine ZnO sample.

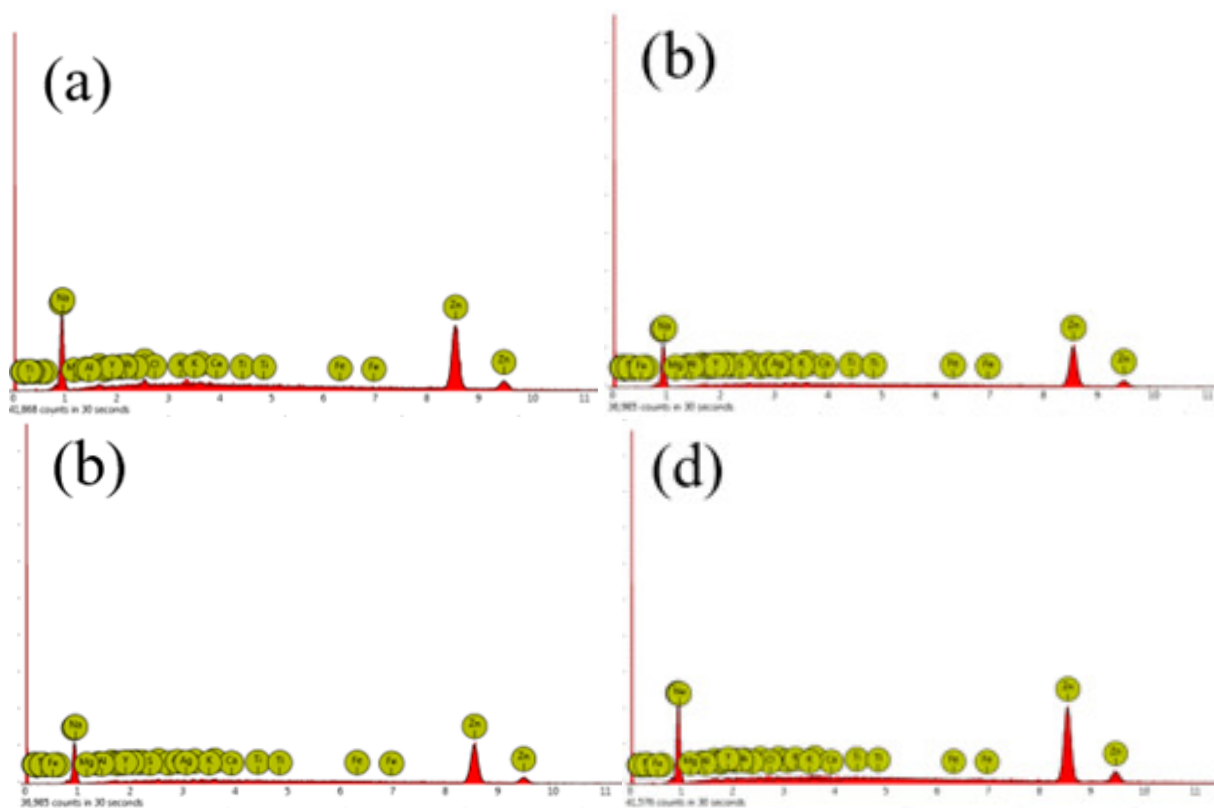


Figure 10: EDX images of (a) the pure ZnO, (b) ZnO with 2AgNPs cycle, (c) ZnO with 4AgNPs cycle, and (d) ZnO with 6AgNPs cycle.

The size of 32 nm shows that the ZnO is mesoporous and it can allow infiltration of the silver NPs in its pores. Addition of different cycle of silver nanoparticles resulted in an increased aggregation of the nanoparticles, as shown in Figures 8b-d. This aggregation may be an indication that the film has grown by a cluster by cluster mechanism and greater sensitivity to the composition of the sample than was possible without AgNPs. Comparison of the micrograph of the films with silver nanoparticles and that without AgNPs reveals changes occurred in the microscopic structure of the film. The silver nanoparticles modified zinc oxide results to nucleation with much film coverage of the substrate surface. The modified surface became dense and brighter which indicates the capability of AgNPs to induce a scattering effect to improve absorptivity of photon energy.

Ag-NPs easily aggregated and formed islands as shown in Figures 8b-d.

A greater degree of aggregation of the particles was seen in photoanode with 6 cycle of AgNPs which could likely not attach well in specific sites on the ZnO surface, resulting in decrease of catalytic activity. The smaller islands in Figure 8b appeared that the formation of a well-structured film on the surface may provide nucleation sites for the formation of the growing film, and may enable greater adhesion of the film to the substrate surface.

Figure 8(e) shows SEM image of the quantum sized AgNPs. The SEM shows high-density AgNPs synthesized. It shows spherical and uniform silver nanoparticles were formed as aggregates with average size of 5 nm as obtained from ISolution Image Analyzer. Most of the silver nanoparticles were roughly circular in shape with smooth edges. It was also observed that grains of the silver modified photoanodes are larger than that of the pure ZnO NPs as shown from the result obtained from image software in Figure 9. The larger grains show initialization of grain stability and boundaries that can encourage recombination is minimized.

The composition of the elements of the formed photoanodes using the SEM electrons, was measured using EDX. The graphical representations of the EDX analyses of the films deposited are presented in Figures 10 (a)-(d). These show the presence of a range of elements, including zinc, sodium, silver, calcium, iron, chlorine, niobium, silicon,

Table 1: Composition of (a) the pure ZnO, (b) ZnO with 2AgNPs cycle, (c) ZnO with 4AgNPs cycle, and (d) ZnO with 6AgNPs cycle.

Element Number	Element Symbol	Element Name	Atomic Conc.	Weight Conc.
30	Zn	Zinc	51.72	74.57
11	Na	Sodium	44.49	22.56
17	Cl	Chlorine	0.92	0.72
14	Si	Silicon	0.61	0.38
12	Mg	Magnesium	0.70	0.38
20	Ca	Calcium	0.38	0.33
41	Nb	Niobium	0.14	0.28
39	Y	Yttrium	0.09	0.18
15	P	Phosphorus	0.21	0.14
26	Fe	Iron	0.10	0.12
13	Al	Aluminium	0.20	0.12
16	S	Sulfur	0.11	0.08
19	K	Potassium	0.08	0.06
7	N	Nitrogen	0.15	0.05
6	C	Carbon	0.10	0.03
22	Ti	Titanium	0.00	0.00

Element Number	Element Symbol	Element Name	Atomic Conc.	Weight Conc.
30	Zn	Zinc	54.09	75.56
11	Na	Sodium	41.87	20.56
47	Ag	Silver	0.33	0.77
20	Ca	Calcium	0.72	0.62
41	Nb	Niobium	0.31	0.61
17	Cl	Chlorine	0.61	0.46
19	K	Potassium	0.46	0.38
39	Y	Yttrium	0.12	0.22
14	Si	Silicon	0.35	0.21
16	S	Sulfur	0.25	0.17
12	Mg	Magnesium	0.27	0.14
13	Al	Aluminium	0.21	0.12
15	P	Phosphorus	0.14	0.09
6	C	Carbon	0.15	0.04
7	N	Nitrogen	0.10	0.03
22	Ti	Titanium	0.00	0.00
26	Fe	Iron	0.00	0.00

Element Number	Element Symbol	Element Name	Atomic Conc.	Weight Conc.
30	Zn	Zinc	53.40	75.18
11	Na	Sodium	41.95	20.77
47	Ag	Silver	0.31	0.73
20	Ca	Calcium	0.56	0.48
26	Fe	Iron	0.33	0.40
17	Cl	Chlorine	0.45	0.34
41	Nb	Niobium	0.16	0.31
14	Si	Silicon	0.51	0.31
13	Al	Aluminium	0.47	0.27
39	Y	Yttrium	0.14	0.27
16	S	Sulfur	0.32	0.22
12	Mg	Magnesium	0.39	0.20
19	K	Potassium	0.23	0.19
22	Ti	Titanium	0.10	0.10
6	C	Carbon	0.37	0.10
7	N	Nitrogen	0.24	0.07
15	P	Phosphorus	0.08	0.06

Element Number	Element Symbol	Element Name	Atomic Conc.	Weight Conc.
30	Zn	Zinc	55.22	76.28
11	Na	Sodium	40.74	19.79
47	Ag	Silver	0.38	0.86
41	Nb	Niobium	0.28	0.55
20	Ca	Calcium	0.56	0.47
39	Y	Yttrium	0.19	0.35
19	K	Potassium	0.40	0.33
17	Cl	Chlorine	0.43	0.32
15	P	Phosphorus	0.41	0.27
14	Si	Silicon	0.34	0.20
12	Mg	Magnesium	0.31	0.16
16	S	Sulfur	0.22	0.15
13	Al	Aluminium	0.22	0.13
22	Ti	Titanium	0.08	0.08
7	N	Nitrogen	0.11	0.03
6	C	Carbon	0.12	0.03
26	Fe	Iron	0.00	0.00

aluminium, yttrium, cadmium, lead, sulfur, silicon, calcium, aluminium, sulfur, magnetisium, potassium, titanium, carbon, nitrogen and phosphorus. The element number, element symbol, element name, numerical atomic concentration and weight concentration, calculated from these intensities, are given in Table 1(a)-(d).

3.7. Solar Cells Photovoltaic Performance

To show the influence that silver nanoparticles has on the photovoltaic performance of the developed dye sensitized solar cells, devices with silver nanoparticles modification were fabricated as shown in Figure 2.

Table 2: The photovoltaic performance of bare ZnO electrode, (b) ZnO/2Ag electrode, (c) ZnO/4Ag electrode and (d) ZnO/6Ag electrode under 100 mWcm^{-2} .

Device Photoanode	J_{sc} (mAcm^{-2})	V_{oc} (V)	FF	$PCE(\%)$
ZnO	0.477	0.762	0.431	0.156
ZnO/2Ag	0.815	0.767	0.597	0.373
ZnO/4Ag	0.635	0.769	0.594	0.290
ZnO/6Ag	0.572	0.722	0.592	0.244

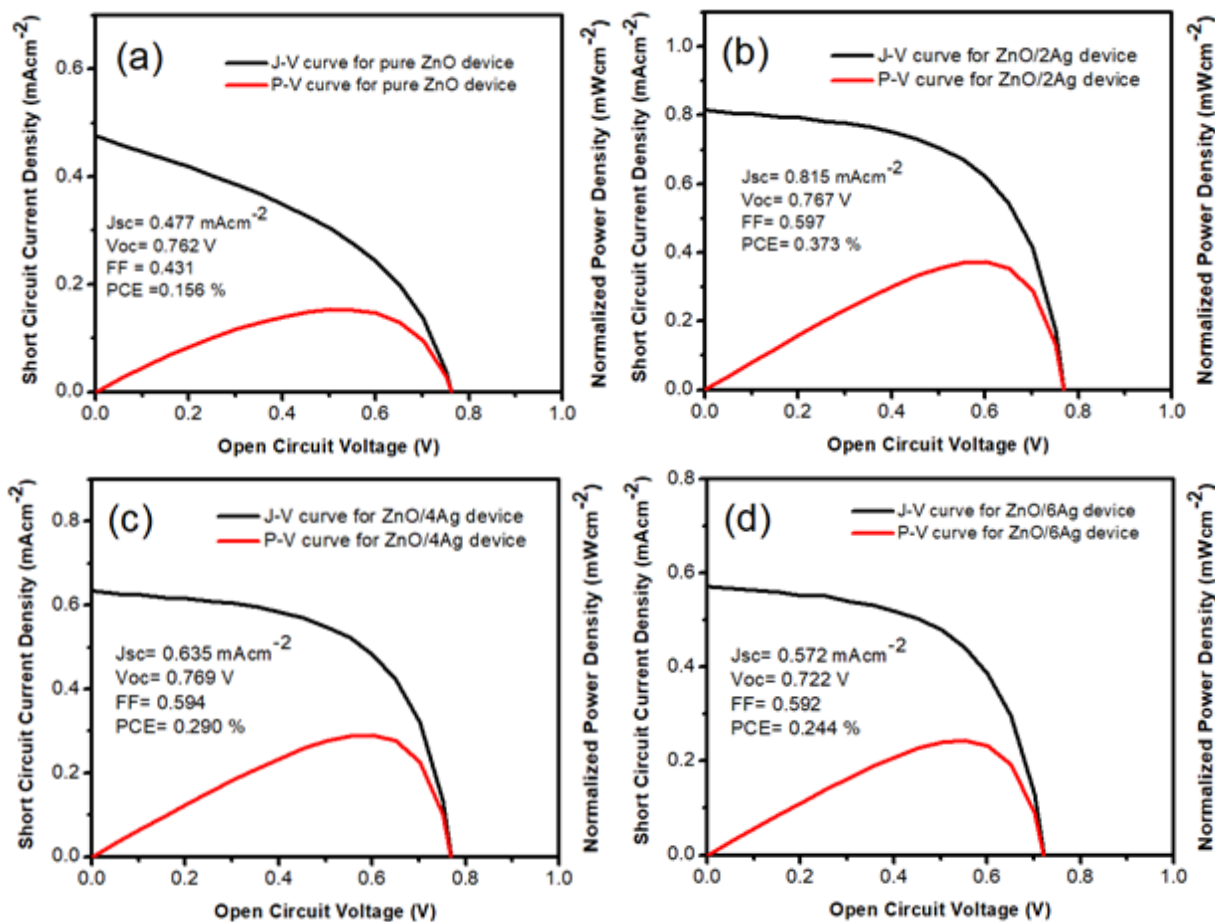


Figure 11: J-V and P-V characteristic curves of DSSCs with (a) bare ZnO electrode, (b) ZnO/2Ag electrode, (c) ZnO/4Ag electrode and (d) ZnO/6Ag electrode.

The open-circuit voltage (V_{oc}), short-circuit current density (J_{sc}), fill factor (FF), and overall conversion efficiency (η) are summarized in Table 2.

As shown from the Table 2, the solar cell based on pure ZnO photoanode demonstrated a PCE of 0.156 %, J_{sc} of 0.477 mAcm^{-2} , V_{oc} of 0.762 V and FF of 0.431. Figure 11 shows that the PCEs of DSSCs with AgNPs was improved as compared with pure ZnO based device.

After depositing 2 cycle of Ag NPs, the short circuit current density increases from 0.477 to 0.815 mAcm^{-2} which results to PCE improvement from 0.156 to 0.373 % showing enhancement of ~ 2.39 times to that of the pristine device. Depositing 4 cycle of AgNPs results to J_{sc} of 0.635 mAcm^{-2} which shows a leading of 0.158 mAcm^{-2} ahead of the reference. As a result, an increase by 85.90 % in PCE has been observed. Also, depositing 6 cycle of AgNPs in

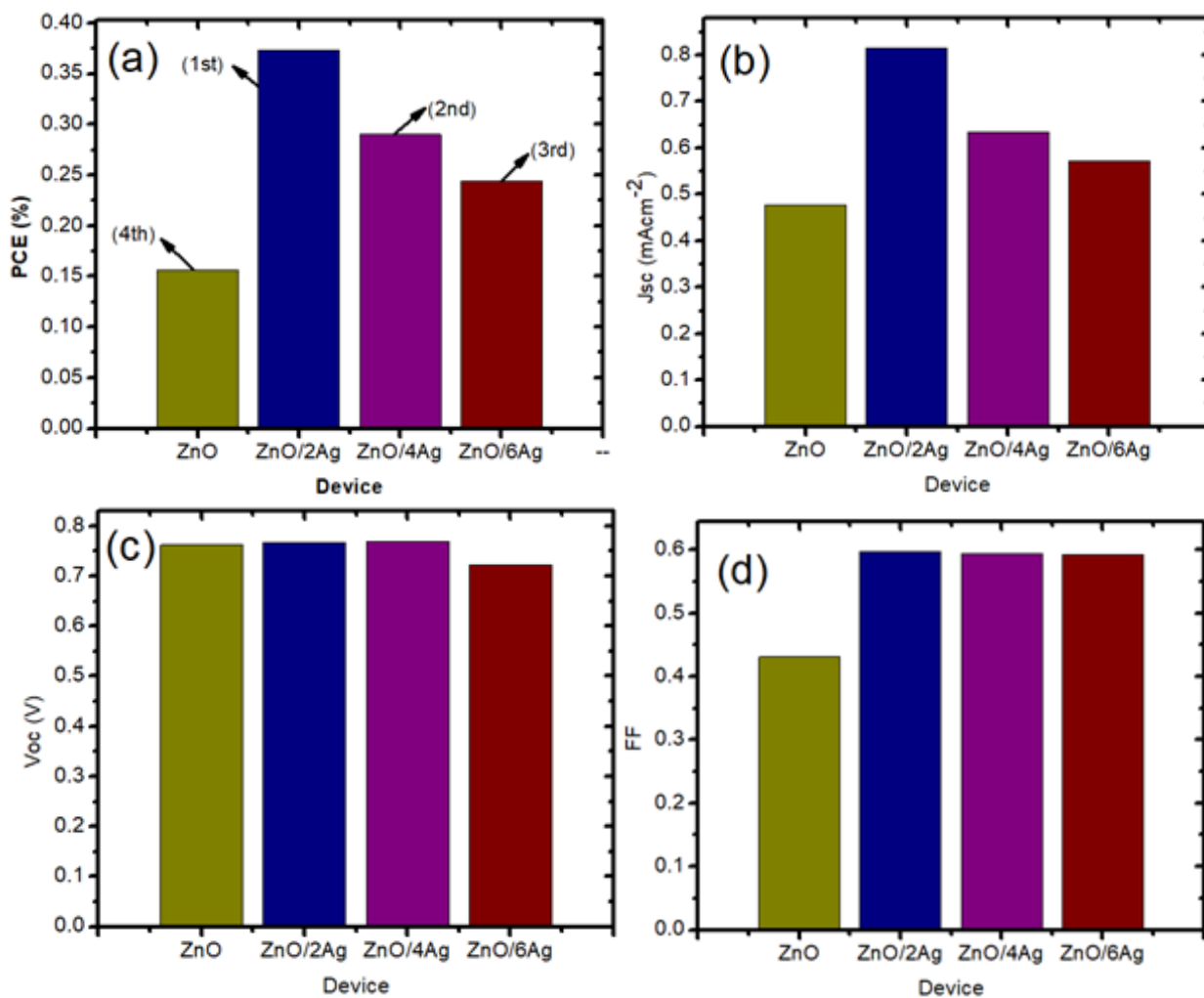


Figure 12: Bar diagrams of the variation in performance parameters of DSSCs with bare ZnO electrode, ZnO/2Ag electrode, ZnO/4Ag electrode and ZnO/6Ag electrode.

the photoanode of bare ZnO NPs results to PCE of 0.244 %, FF of 0.592, Jsc of 0.572 mAcm⁻² and Voc of 0.722 V which also shows an enhancement of ~ 1.56 times, ~ 1.37 times and ~1.20 times in PCE, FF and Jsc over the device lacking AgNPs. This result clearly shows that all devices performance with AgNPs improved. Better performance seen on silver-modified devices can be attributed to a decrease in recombination of electron hole pairs by Ag-Zno junctions. The improved strength in light scattering, decrease in electron transport resistance by trapping, also plays an important role to improve the photosensitive performance observed.

The devices containing 2 cycles of silver nanoparticles shows the best performance. Further increase in the number of cycles degrades the performance. Surprisingly, as the Cycle of AgNP increases, as shown in Figures 8(c) and (d), AgNp is easily agglomerated to form an island, resulting in reduced catalytic activity and decreased performance. The effective surface area is significantly reduced and the number of potential charge trap sites also increases. This reduces the performance of the device since not all the surfaces of the ZnO NPs are evenly coated by the higher number of AgNPs. The introduced nanoparticles also contribute to the improved efficiency by effectively transporting the photoinjected electron from the dye to the composite electrode [15]. A faster electron transport improves the charge collection efficiency, which in turn improves the short circuit current density and PCE.

In the presence of Ag NPs, the absorption range of ZnO extends into the visible region due to the SPR effect. As

a result, the concentration of charge carriers increases greatly [15]. When the visible light strikes the surface of the Ag NPs, the photogenerated electrons from the Fermi level of Ag jumps to the valance band (VB) of ZnO. In the presence of UV irradiation, the photogenerated electrons from the VB of ZnO transfer to the conduction band (CB) of the ZnO. The enhanced electromagnetic field that is produced in the presence of Ag NPs improves light absorption of dye molecules and thus excites more electrons than usual, same applicable to other semiconductors (TiO₂) [15, 43].

Silver nanoparticles has a large work function which results to a Schottky barrier established at the Ag/ZnO junction [11]. The electric field produced by the barrier promotes the effective separation/dissociation of the optical electron-hole pair. Due to this fact, electrons can effectively pass through the network and reach the electrode, and the hole reaches the electrolyte and then be captured by the specie reduced [15]. Further, this can be explained by the energy level of the photoanode material, and therefore: lowest unoccupied molecular orbital (LUMO) of the mixed dye molecules has electrons that can then be moved to Ag NPS and the CB of ZnO.

Because of the electron approach, the Fermi level of the Ag shifts towards more negative potential until it comes closer to the Fermi level of the ZnO NPs. Due to surface plasmon resonance exhibited by the Ag, it enhanced electron capturing and storage capability resulting from Ag-NP thereby reducing quenching losses and the PCE is increased [16, 17, 36]. Figure 12 shows the photovoltaic parameters (PCE, Jsc, Voc and FF) of the four cells against the fabricated devices. The plots show the best PCE, Jsc and FF with the device with 2 cycles of silver nanoparticles and the best Voc was observed in device with 4 cycles of AgNPs.

4. Conclusion

By simply introducing quantum-sized AgNP into DSSC active layer, we recorded an improved photoanode of DSSC made of ZnO nanoparticles. The presence of AgNP produced a surface plasmon resonance effect that led to an increase in the devices. Ag nanoparticles serve to enhance dye absorption and light scattering within the device, improving charge collection efficiency by providing a preferred electron path. AgNP was deposited in cycles (2 cycles, 4 cycles, and 6 cycles). Maximum efficiency was recorded on device with 2 cycles of AgNP, giving PCE of 0.373%, Jsc of 0.815 mAcm⁻², Voc of 0.767 V, and FF of 59.7%. These results show a 70.86% and 139.10% improvement in Jsc and PCE over devices without AgNP.

References

- [1] G. Yirga, S. Tadesse & T. Yohannes, "Photoelectrochemical Cell Based on Natural Pigments and ZnO Nanoparticles", *Journal of Energy and Natural Resources* **5** (2016) 1.
- [2] S. Sreeja & B. Pesala, "Plasmonic enhancement of betanin-lawsone co-sensitized solar cells via tailored bimodal size distribution of silver nanoparticles", *Scientific Reports* **10** (2020) 8240.
- [3] H. Nan, H. Shen, G. Wang, S-D. Xie, G-J. Yang & H. Lin, "Studies on the optical and photoelectric properties of anthocyanin and chlorophyll as natural co-sensitizers in dye sensitized solar cell.", *Optical Materials* **73** (2017) 172.
- [4] E. Danladi, P. M. Gyuk & E. B. Danladi, "Chlorophyll and Betalain as Light-Harvesting Pigments for Nanostructured TiO₂ Based Dye-Sensitized Solar Cells", *Journal of Energy and Natural Resources*, **5** (2016) 53.
- [5] M. A. M. Al-Alwani, N. A. Ludin, A. B. Mohamad, A. A. H. Kadhum & K. Sopian, "Extraction, preparation and application of pigments from Cordyline fruticosa and Hylocereus polyrhizus as sensitizers for dye-sensitized solar cells", *Spectrochimie Acta - Part A Molecular and Biomolecular Spectroscopy* **179** (2017) 23.
- [6] G. Richhariya, A. Kumar, P. Tekasakul & B. Gupta, "Natural dyes for dye sensitized solar cell: A review", *Renewable and Sustainable Energy Reviews* **69** (2017) 705.
- [7] C. Sandquist & J. L. McHale, "Improved efficiency of betanin-based dye-sensitized solar cells", *Journal of Photochemistry and Photobiology A: Chemistry* **221** (2011) 90.
- [8] R. Ramamoorthy, N. Radha, G. Maheswari, S. Anandan, S. Manoharan & R. V. Williams, "Betalain and anthocyanin dye-sensitized solar cells", *Journal of Applied Electrochemistry* **46** (2016) 929.
- [9] S. A. M. Al-Bat'hi, I. Alaei & I. Sopyan, "Natural photosensitizers for dye sensitized solar cells", *International Journal of Renewable Energy Research* **3** (2013) 138.
- [10] S. Kim, M. Jahandar, J. H. Jeong & D. C. Lim, "Recent Progress in Solar Cell Technology for Low-Light Indoor Applications", *Current alternative energy* **3** (2019) 3.
- [11] D. Eli, G. J. Ibeh, O. O. Ige, J. A. Owolabi, R. U. Ugbe, B. O. Sherifdeen, M. Y. Onimisi & H. Ali "Silver Nanoparticles as Nano Antenna for TiO₂ Activation and its Application in DSSC for Enhanced Performance", *Physics Memoir:Journal of Theoretical and Applied Physics* **1** (2019) 88.
- [12] M. R. Narayan, "Review: Dye sensitized solar cells based on natural photosensitizers", *Renewable and Sustainable Energy Reviews* **16** (2012) 208.

- [13] I. D. Costa-Rocha, B. Bonnlaender, H. Sievers, I. Pischel & M. Heinrich, "Hibiscus sabdariffa L. – A phytochemical and pharmacological review", *Food Chemistry*, **165** (2014) 424.
- [14] J. A. Bonacin, F. M. Engelmann, D. Severino, H. E. Toma & M. S. Baptista, "Singlet Oxygen Quantum Yields (φ_{Δ}) in Water using Beetroot Extract and an Array of LEDs", *Journal of the Brazilian Chemical Society* **20** (2009) 31.
- [15] B. D. Choudhury, C. Lin, S. M. Z. Shawon, J. S. Martinez, H. Huq & M. J. Uddin, "A photoanode with hierarchical nanoforest TiO₂ structure and silver plasmonic nanoparticles for flexible dye sensitized solar cell", *Scientific Reports* **11** (2021) 7552.
- [16] E. Danladi & P. M. Gyuk, "High Efficiency Dye Sensitized Solar Cells by Excitation of Localized Surface Plasmon Resonance of AgNPs", *Science World Journal* **14** (2019) 125.
- [17] M. Y. Onimisi, E. Danladi, S. G. Abdu, H. O. Aboh & E. Jonathan, "Size Effects of Silver Nanoparticles on the Photovoltaic Performance of Dye Sensitized Solar Cells", *American Chemical Science Journal* **13** (2016) 1.
- [18] Q. Wali, A. Fakharuddin & R. Jose, "Tin oxide as a photoanode for dye-sensitized solar cells: Current progress and future challenges", *Journal of Power Sources* **293** (2015) 1039.
- [19] S. Khadtare, A. S. Ansari, H. M. Pathan, S. H. Han, K. M. Mahadevan, S. D. Mane & C. Bathula, "Silver nanoparticles loaded ZnO photo-electrode with Rose Bengal as a sensitizer for dye sensitized solar cells", *Inorganic Chemistry Communications* **104** (2019) 155.
- [20] V. F. Nunes, A. P. S. Souza, F. Lima, G. Oliveira, F. N. Freire & A. F. Almeida, "Effects of Potential Deposition on the Parameters of ZnO dye-sensitized Solar Cells", *Materials Research* **21** (2018) 1.
- [21] L. P. Joshi, Y. Poudel, M. L. Nakarmi, P. R. Niraula & S. P. Shrestha, "Preparation and Characterization of Zinc Oxide Based Photoanode for Dye-sensitized Solar Cell using Delonix Regia Natural Dye Extract", *Journal of Nepal Physical Society* **4** (2017) 1.
- [22] N. Kicir, T. Tüken, O. Erken, C. Gumus & Y. Ufuktepe, "Nanostructured ZnO films in forms of rod, plate and flower: Electrodeposition mechanisms and characterization", *Applied Surface Science* **377** (2016) 191.
- [23] J. Hofmann & W. Steinman, "Plasma resonance in photoemission of silver", *Physica Status Solidi* **30** (1968) 53.
- [24] J. G. Endriz & W. E. Spicer, "Surface-plasmon-one-electron decay and its observation in photoemission", *Physical Review Letters* **24** (1970) 64.
- [25] E. Danladi, M. Ahmad, I. Maxwell, D. Ezra, A. Francis & S. Sarki, "Dye-Sensitized Solar Cells Using Natural Dyes Extracted from Roselle (*Hibiscus Sabdariffa*) Flowers and Pawpaw (*Carica Papaya*) Leaves as Sensitizers", *Journal of Energy and Natural Resources* **5** (2016) 11.
- [26] B. C. Mphande & A. Pogrebnoi, "Outdoor Photoelectrochemical Characterization of Dyes from *Acalypha wilkesiana* 'Haleakala' and *Hibiscus sabdariffa* as Dye Solar Cells Sensitizers" *British Journal of Applied Science & Technology* **7** (2015) 195.
- [27] H.K. Jun, M.A. Careem & A.K. Arof, "Plasmonic effects of quantum size gold nanoparticles on dye-sensitized solar cell, 5th International Conference on Functional Materials & Devices (ICFMD 2015)", *Materials Today: Proceedings* **3S** (2016) S73.
- [28] M. Mrad, B. Chouchene & T. B. Chaabane, "Effects of Zinc Precursor, Basicity and Temperature on the Aqueous Synthesis of ZnO Nanocrystals", *South African journal of chemistry*, **71** (2018) 103.
- [29] S. Xu & Z. L. Wang "One dimensional ZnO nanostructures: solution growth and functional properties", *Nano research* **4** (2011) 1013.
- [30] D. Eli, M. Y. Onimisi, S. Garba & J. Tasiu, "9.05 % HTM free perovskite solar cell with negligible hysteresis by introducing silver nanoparticles encapsulated with P₄VP Polymer, *SN Applied Sciences* **2** (2020) 1769
- [31] S. Agnihotri, S. Mukherji & S. Mukherji, "Size-controlled silver nanoparticles synthesized over the range 5–100 nm using the same protocol and their antibacterial efficacy", *RSC Advances* **4** (2014) 3974.
- [32] A. Dumbravă, I. Enache, C. I. Oprea, A. Georgescu & M. A. Gîrțu, "Toward a more efficient utilisation of betalains as pigments for Dye-Sensitized solar cells" *Digest Journal of Nanomaterials and Biostructures* **7** (2012) 339.
- [33] N. Ruba S. Sowmya, P. Pooja, B. Janarthanan & P. A. Nagamani Prabu, "Dye-Sensitized Solar Cells Using a Cocktail of Synthetic (Eosin Y) and Natural (Beetroot, Pomegranate, and Kumkum) Dyes", *Brazilian Journal of Physics* **51** (2021) 1459.
- [34] K. R. Chethan, Y. R. Mohammed, R. Mohammed, K. Y. Ramesh & K. Hemant, "Extraction of Betalain Dye from Beetroot and Preparation of Organic DSSC", *International Journal of Scientific & Engineering Research* **11** (2020) 165.
- [35] M. J. García-Salinas & M. J. Ariza, "Optimizing a Simple Natural Dye Production Method for Dye-Sensitized Solar Cells: Examples for Betalain (Bougainvillea and Beetroot Extracts) and Anthocyanin Dyes", *Applied Sciences* **9** (2019) 2515.
- [36] K. Guo, M. Li, X. Fang, X. Liu, B. Sebo, Y. Zhu, Z. Hu & X. Zhao, "Preparation and enhanced properties of dye-sensitized solar cells by surface plasmon resonance of Ag nanoparticles in nanocomposite photoanode", *Journal of power sources* **203** (2012) 155.
- [37] Y. M. Yeh, Y. S. Wang & J. H. Li, "Enhancement of the optical transmission by mixing the metallic and dielectric nanoparticles atop the silicon substrate", *Optics Express* **19** (2011) A80.
- [38] T. J. Antosiewicz & T. Tarkowski, "Localized surface plasmon decay pathways in disordered two-dimensional nanoparticle arrays", *ACS Photonics* **2** (2015) 1732.
- [39] N. Pazos-Perez, C. S. Wagner, J. M. Romo-Herrera, L. M. Liz-Marzan, F. J. Garcia de Abajo, A. Wittemann, A. Fery & A. Alvarez-Puebla, "Organized plasmonic clusters with high coordination number and extraordinary enhancement in surface-enhanced raman scattering (SERS)", *Angew Chemie* **51** (2012) 12688.
- [40] F. L. Yap, P. Thoniyot, S. Krishnan & S. Krishnamoorthy, "Nanoparticle cluster arrays for high-performance through directed self-assembly on flat substrates and on optical fibers", *ACS Nano* **6** (2012) 2056.
- [41]] F. M. Mohammadi & N. Ghasemi, "Influence of temperature and concentration on biosynthesis and characterization of zinc oxide nanoparticles using cherry extract", *Journal of Nanostructure in Chemistry* **8** (2018) 93.
- [42] B. Timothy, J. William, P. Alexandra, S. Ewa & P. Jerzy, "The role of anhydrous zinc nitrate in the thermal decomposition of the zinc hydroxy nitrates Zn₅(OH)₈(NO₃)₂·2H₂O and ZnOHNO₃·H₂O", *Journal of Solid State Chemistry* **180** (2007) 1171.
- [43] H. Hu, J. Shen, X. Cao, H. Wang, H. Lv, Y. Zhang, W. Zhu, J. Zhao & C. Cui, "Photo-assisted deposition of Ag nanoparticles on branched TiO₂ nanorod arrays for dye-sensitized solar cells with enhanced efficiency", *Journal of Alloy and Compound* **694** (2017) 653.